Bare electron dispersion from experiment: Self-consistent self-energy analysis of photoemission data

A. A. Kordyuk,[1,2] S. V. Borisenko,[1] A. Koitzsch,[1] J. Fink,[1] M. Knupfer,[1] and H. Berger[3]
[1]*Institute for Solid State Research, IFW-Dresden, Helmholtzstrasse 20, D-01069 Dresden, Germany*
[2]*Institute of Metal Physics of National Academy of Sciences of Ukraine, 03142 Kyiv, Ukraine*
[3]*Institute of Physics of Complex Matter, EPFL, CH-1015 Lausanne, Switzerland*
(Received 27 December 2004; published 9 June 2005)

Performing an in-depth analysis of the photoemission spectra along the nodal direction of the high-temperature superconductor Bi-2212 we developed a procedure to determine the underlying electronic structure and established a precise relation of the measured quantities to the real and imaginary parts of the self-energy of electronic excitations. The self-consistency of the procedure with respect to the Kramers-Kronig transformation allows us to draw conclusions on the applicability of the spectral function analysis and on the existence of well-defined quasiparticles along the nodal direction even for the underdoped Bi-2212 in the pseudogap state. The analysis of the real part of the self-energy $\Sigma'(\omega)$ for an overdoped and underdoped Bi-2212 helps to distinguish the 70 meV "kink" from $\Sigma'(\omega)$ maximum and conclude about doping dependence of the kink strength.

DOI: 10.1103/PhysRevB.71.214513 PACS number(s): 74.25.Jb, 71.15.Mb, 74.72.Hs, 79.60.−i

I. INTRODUCTION

With modern angle-resolved photoemission spectroscopy[1,2] (ARPES) one gets a direct snapshot of the density of low-energy electronic excited states in the momentum-energy space of two-dimensional (2D) solids.[3–6] All the interactions of the electrons which are responsible for the unusual normal and superconducting properties of cuprates are encapsulated in such pictures, but are still hard to decipher. One way to take into account these interactions is to consider electronic excitations as quasiparticles which, compared to the noninteracting electrons, are characterized by an additional complex self-energy.[7] Extraction of the self-energy from experiment is thus of great importance to check the validity of the quasiparticle concept and understand the nature of interactions involved, but appears to be problematic since the underlying band structure of the bare electrons is *a priori* unknown.

One can evaluate the interaction parameters taking the bare band dispersion from band structure calculations,[4] however, this unavoidably increases the uncertainty of any conclusions on the strength and nature of the interactions involved. A direct determination of the bare band structure from experiment would be much more attractive in this sense. Previously, the bare band dispersion has been assigned to the high binding energy part of the experimental dispersion.[8] In Refs. 9 and 10 we have discussed that the bare Fermi velocity estimated from the nodal ARPES spectra using the Kramers-Kronig (KK) transformation is in reasonable agreement with band structure calculations[11,12] and with an analysis of the anisotropic plasmon dispersion,[13] although it has been pointed out that in order to quantify interaction parameters such as coupling strength[14] or self-energy[15] a precise and reliable approach of bare band determination is needed.

In this paper we introduce an approach to directly extract both the bare band dispersion and the self-energy functions from ARPES spectra. We show that the approach is self-consistent within the highest experimental accuracy available today. Applying the procedure to the spectra from the underdoped and overdoped Bi(Pb)-2212 as well as for optimally doped Bi(La)-2201, we demonstrate the validity of the quasiparticle concept in cuprates even in the pseudogap state.

II. NODAL SPECTRA ANALYSIS

We start with a brief overview of the basics of the nodal spectra analysis within the self-energy approach. Measuring the photoemission intensity as a function of the kinetic energy and in-plane momentum of outgoing electrons $I(E_k,\mathbf{k})$ one obtains access to the spectral function of the one electron removal which is supposed to reflect the quasiparticle properties of the remaining photohole: its effective mass and lifetime. These properties can be expressed in terms of a quasiparticle self-energy $\Sigma=\Sigma'+i\Sigma''$, an analytical function the real and imaginary parts of which are related by the KK transformation (see Sec. 1 of the Appendix). Neglecting for the moment the effects of the energy and momentum resolutions as well as the influence of matrix elements,[6] one can take $I\propto A(\omega,\mathbf{k})$, where ω is the energy of the remaining photohole with respect to the Fermi level. In turn, the spectral function can be formulated in terms of the self-energy

$$A(\omega,\mathbf{k}) = -\frac{1}{\pi}\frac{\Sigma''(\omega)}{[\omega-\varepsilon(\mathbf{k})-\Sigma'(\omega)]^2+\Sigma''(\omega)^2}, \qquad (1)$$

where $\varepsilon(\mathbf{k})$ is the bare band dispersion. Within such a definition, $\Sigma''(\omega)<0$, and $\Sigma'(\omega)>0$ for $\omega<0$.

A. Linear dispersion

In case there is no interaction, i.e. electronic excitations can live forever, the spectral function is a delta function with the pole $\omega-\varepsilon(\mathbf{k}_\omega)=0$ and, e.g., for the nodal direction, can be

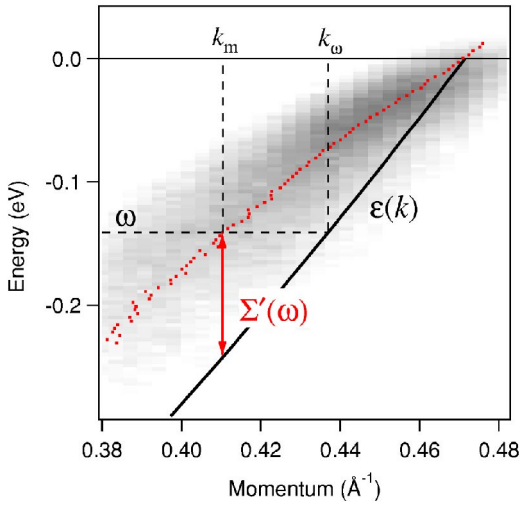

FIG. 1. (Color online.) Bare band dispersion (solid line) and renormalized dispersion (points) on top of the spectral weight of interacting electrons. Though intended to be general, this sketch represents the nodal direction of an underdoped Bi-2212.

represented by the solid line in Fig. 1. When interactions are present, the self-energy leads to a shifting and broadening of the noninteracting spectral function. The resulting picture is essentially that which is measured in ARPES (the blurred region in Fig. 1 illustrates this). If one neglects the momentum dependence of the self-energy, then, from Eq. (1), the momentum distribution curves $[\mathrm{MDC}(k)=A(k)_{\omega=\mathrm{const}}]$ have maxima at $k_m(\omega)$ determined by $\omega-\varepsilon(k_m)-\Sigma'(\omega)=0$ for a given ω. In other words, $\Sigma'(\omega)=\omega-\varepsilon(k_m)$, is that which is illustrated in Fig. 1 by the double-headed arrow. In the region where the bare dispersion can be considered as linear (with a slope v_F) one can write

$$\Sigma'(\omega) = \omega - v_F[k_m(\omega) - k_F]. \tag{2}$$

Assuming in addition weak **k** dependence of Σ'' along a cut perpendicular to the Fermi surface (see discussion in Sec. 5 of the Appendix), the MDCs exhibit a Lorentzian line shape[5] with the half width at half maximum W and

$$\Sigma''(\omega) = -v_F W(\omega). \tag{3}$$

Thus, the determination of both the real and imaginary parts of the self-energy requires the knowledge of the bare dispersion $\varepsilon(k)$ (or, in the vicinity to E_F, an "energy scale," e.g., Fermi velocity v_F).[9] The KK transformation gives an additional equation which relates these functions: $\Sigma'=\mathrm{KK}\Sigma''$ [e.g., Eq. (A1)]. This opens the way to extract all desired quantities from the experiment, but brings a new "problem of tails." Under "tails" we mean the behavior of $\Sigma''(\omega)$ for energies $|\omega|>\omega_m$, where ω_m is a "confidence limit," a maximal experimental binding energy to which both the $W(\omega)$ and $k_m(\omega)$ functions can be confidently determined.

Fortunately, as we show in Sec. 3 of the Appendix, the different but reasonable tails of $\Sigma''(\omega)$ almost do not effect the low-energy behavior of $\Sigma'(\omega)$. The influence of the high-energy region on the coupling strength (A3) can be described by mainly one parameter, the high-energy cutoff ω_c. This gives us the way to solve the whole problem, examining a wider energy range of the ARPES data.

B. Quadratic dispersion

One more complication should be addressed here: in the wider energy range a deviation of the bare dispersion from a line should be taken into account. Along the nodal direction the TB band in the occupied part can be well approximated by a simple parabola $\varepsilon(k)=\omega_0(1-k^2/k_F^2)$,[9] for which we still need one energy scale parameter: the bottom of the bare band ω_0 or the bare Fermi velocity $v_F=-2\omega_0/k_F$. Using this dispersion in Eq. (1), one can finally modify Eqs. (2) and (3) to

$$\Sigma'(\omega) = \frac{v_F}{2k_F}[k_m^2(\omega) - k_F^2] + \omega, \tag{4}$$

$$\Sigma''(\omega) = -\frac{v_F}{k_F} W(\omega)\sqrt{k_m^2(\omega) - W^2(\omega)}. \tag{5}$$

C. Fitting procedure

In short, the fitting machinery is based on Eqs. (4), (5), and (A1). One can define three steps here. In the two first steps, the real part of the self-energy, for given ω_0, ω_c, and n (which characterizes the tails, see below), is calculated in two ways (i) Σ'_{disp} by Eq. (4), (ii) Σ'_{KK} by Eq. (5) with subsequent KK transform (A1). Then, in step (iii), the parameters ω_0, ω_c, and n [see Eq. (A11)] are varied until $\Sigma'_{\mathrm{disp}}(\omega)$ and $\Sigma'_{\mathrm{KK}}(\omega)$ coincide. In practice, we fit the difference $\Sigma'_{\mathrm{disp}}-\Sigma'_{\mathrm{KK}}$ to a small contribution of experimental resolution. The details of the procedure are given in Secs. 3 and 4 of the Appendix.

III. RESULTS

We have applied the described procedure to the experimental data measured along the nodal direction for the following samples: underdoped Bi(Pb)-2212 ($T_c=77$ K), overdoped ($T_c=75$ K) Bi(Pb)-2212, and optimally doped Bi(La)-2201 ($T_c=32$ K), marked in the following as UD77, OD75, and OP32, respectively. The data for UD77 and OD75 were collected at 130 K, and for OP32 at 40 K. We have explored a number of excitation energies in the range of 17–55 eV but, as we show below, only at 27 eV, at which only the antibonding band is visible,[12] the described procedure can be directly applied to the bilayer Bi samples. The experimental details can be found elsewhere.[14,15]

Figure 2 illustrates an example of the ARPES spectrum, photocurrent as a function of energy and momentum, taken for UD77 Bi(Pb)-2212 at 130 K along the nodal direction. On top of it, we plot the result of the fitting procedure, the bare dispersion.

Another result of the procedure is the self-energy functions. They are shown in Fig. 3 for UD77 and in Fig. 4 for OD75 and OP32. We remind that the real part of the self-energy is represented by two functions Σ'_{disp} and Σ'_{KK}, obtained, as it is described above, from the experimental dis-

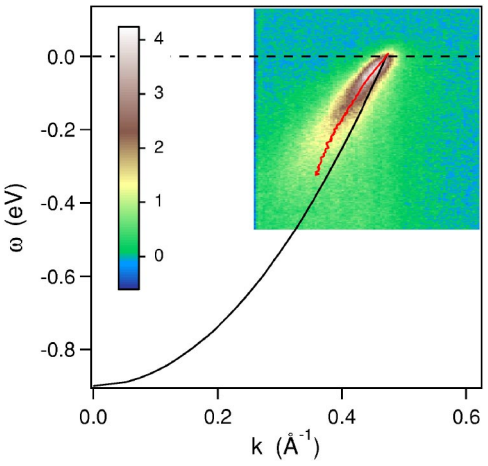

FIG. 2. (Color online.) The bare band dispersion along the nodal direction of an underdoped Bi(Pb)-2212 (solid parabola) on top of its spectral weight at 130 K measured by ARPES. MDC (or renormalized) dispersion shown by solid white (red) line.

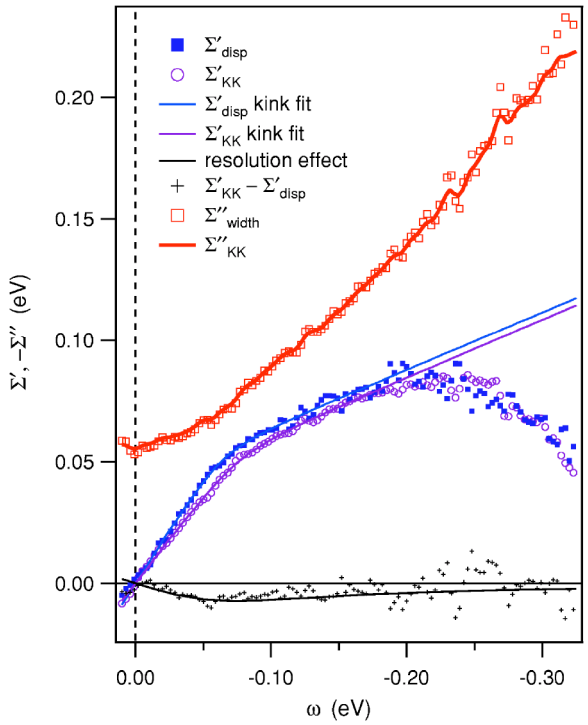

FIG. 3. (Color online.) Real and imaginary parts of the self-energy extracted from the experiment with the described procedure. A complete coincidence between the corresponding parts of the self-energy calculated from the two different experimental functions, the MDC dispersion and MDC width, demonstrates the full self-consistency of the ARPES data treated within the self-energy approach.

persion by Eq. (4) and from MDC widths with subsequent KK transform, respectively. The irreducible difference $\Sigma'_{\mathrm{disp}} - \Sigma'_{\mathrm{KK}}$ and the resolution function $R'(\omega)$, to which the difference is fitted, are also shown. Consequently, the interaction parameters which we give below should be referred to the Σ'_{disp} functions.

The imaginary part of the self-energy is presented by $\Sigma''_{\mathrm{width}}(\omega)$ function defined by Eq. (5). In order to check the correctness of the KK numerics, we also plot the $\Sigma''_{\mathrm{KK}}(\omega)$ function which is obtained by back KK-transform (A2) of $\Sigma'_{\mathrm{KK}}(\omega)$.

The complete coincidence of Σ'_{disp} and $\Sigma'_{\mathrm{KK}} - R'$ functions in the whole accessible energy range substantiates that the self-energy constructed using Eqs. (4) and (5) is self-consistent within the experimental accuracy currently available with ARPES. This self-consistency shows, in addition to the applicability of the self-energy approach to superconducting cuprates, that the measured spectra belong to a single band and are free of influence of any unaccounted additional features such as other bands, superstructures, or *k*-dependent backgrounds. It has been shown recently[12] that although the electronic dispersion along the nodal direction in the bilayer Bi-2212 is not degenerated, i.e., has a finite splitting about 0.05 eV for the bare dispersion, the photoemission from the bonding band is highly suppressed at exactly 27 eV excitation energy. At other energies we do not expect that the described fitting procedure will work if applied directly. Figure 4(b) demonstrates this showing the "best" fitting result that can be achieved for $h\nu = 38$ eV. The difference between $\Delta\Sigma'(\omega)$ and $R'(\omega)$ is apparent. At these "inconvenient" energies the contributions of each band should be separated first, that complicates the analysis but can be done in principle by measuring several spectra at different $h\nu$ or polarization (e.g., see Ref. 16).

In Table I we give the values of the experimental and calculated parameters for three investigated samples, for which the self-energy functions are shown in Figs. 3, 4(a), and 4(c). The Fermi momentum k_F and the renormalized Fermi velocity v_R are determined experimentally; the energy of the bottom of the bare band ω_0, the bare Fermi velocity v_F, and the coupling strength λ are the results of the fitting procedure.

Other fitting parameters, which characterize the high-energy tails of $\Sigma''(\omega)$, are not so well defined as ω_0 and λ for the reasons we discuss in Secs. 3 and 4 of the Appendix, but we can state that $|\omega_c| \approx |\omega_0|/2$. In case of the OD sample, the parameters $\omega_c = 0.40 \pm 0.05$ eV, $n = 4 \pm 0.5$ are better determined because of a higher confidence limit $\omega_m = 0.45$ eV at which one can see that $\Sigma''(\omega)$ starts to saturate (Sec. IV B).

IV. DISCUSSION

The presented examples purpose to illustrate the applicability of the self-energy approach to Bi-cuprates. We believe that the described procedure gives a powerful technique to purify the ARPES data from artificial features and to build a strong experimental basis for understanding of the nature of electronic interactions in cuprates, but still a big work on the data analysis should be performed. Nevertheless, some conclusions can be made even on this stage.

A. Well-defined quasiparticles

The linear behavior of $\Sigma'(\omega)$ over a wide energy range $|\omega| < |\omega_k|$ indicates, using the criterion $\lim_{\omega \to 0} \Sigma''(\omega)/\omega = 0$,

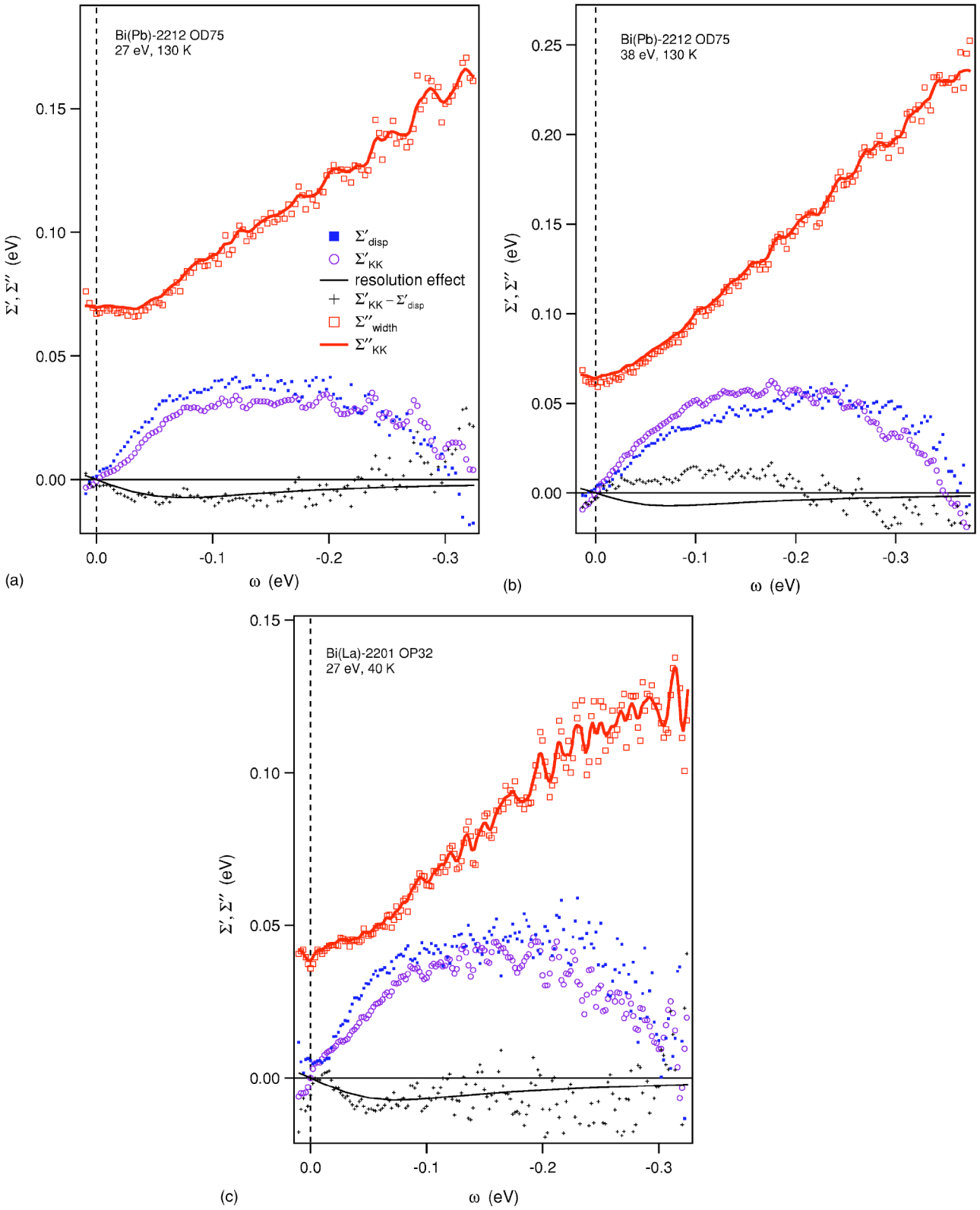

FIG. 4. (Color online.) Real and imaginary parts of the self-energy extracted from the experiment with the described procedure.

the existence of well-defined quasiparticles in the pseudogap state: for the underdoped Bi(Pb)-2212 at 130 K the coherence factor $Z=0.54\pm0.03$. The offset of $\Sigma''(\omega)$ not only comes from finite resolution but also finite temperature and scattering on impurities,[17] which are mostly energy independent[15] and do not contribute to the slope of $\Sigma'(\omega)$ and, therefore, to the coherence factor.

In Ref. 10 we have noticed that the scattering rate at room temperature looks more linear for underdoped samples than for overdoped ones that is in favor of the marginal Fermi

TABLE I. Experimental and calculated parameters of the quasiparticle spectral function along the nodal direction in the normal state for three investigated samples: the Fermi momentum k_F and the renormalized Fermi velocity v_R are determined experimentally; the energy of the bottom of the bare band ω_0, the bare Fermi velocity v_F, and the coupling strength λ are the results of the described fitting procedure.

Sample	k_F (Å^{-1})	v_R (eV Å)	ω_0 (eV)	v_F (eV Å)	λ
Bi(Pb)-2212 UD77	0.471	2.04±0.05	−0.90±0.04	3.82±0.17	0.87±0.12
Bi(Pb)-2212 OD75	0.445	2.46±0.07	−0.86±0.03	3.87±0.14	0.57±0.10
Bi(La)-2201 OP32	0.47	2.04±0.10	−0.79±0.05	3.36±0.22	0.65±0.16

liquid model (MFL).[18] It is important to stress that $\Sigma'(\omega)$, determined with better accuracy, exhibits a linear behavior below and above the kink energy ω_k (see Fig. 2) which is now difficult to reconcile with the MFL model: as far as a slope in $\Sigma'(\omega)$, according to Eq. (A4), is mainly determined by the coefficient at $(\omega-\omega_x)^2$ term in the expansion of $\Sigma''(\omega)$ around ω_x, the straight sections on $\Sigma'(\omega)$ imply the regions where $\Sigma''(\omega)$ is precisely parabolic (exhibits constant curvature over some finite-energy regions).

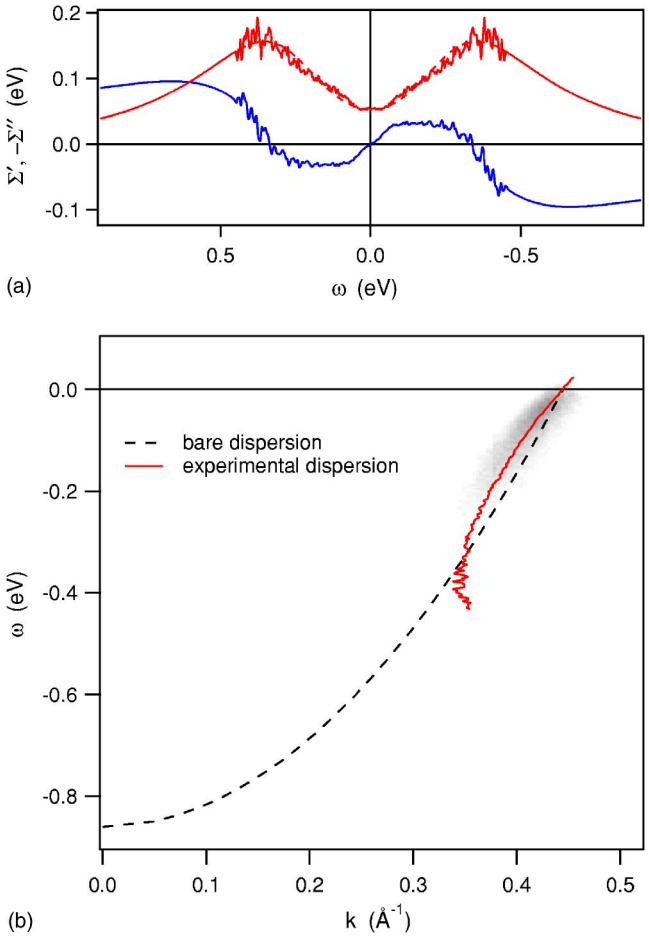

FIG. 5. (Color online.) The results of the fitting procedure for Bi(Pb)-2212 OD75: (a) real (odd curve) and imaginary (even curves) parts of the self-energy; (b) the experimental (solid line) and bare (dashed line) dispersions on top of the experimentally measured quasiparticle spectral weight.

B. High-energy cutoff

It is interesting to note that even for the UD77 sample, for which the saturation of $\Sigma''(\omega)$ has not been observed, it is not possible to reconcile the high-energy behavior of $\Sigma''(\omega)$ with the saturation extreme (A9) [or (A10) with $n=2$]. This means that $|\Sigma''(\omega)|$ reaches the maximum and starts to decrease at about ω_c, and, consequently, $\Sigma'(\omega)$ changes the sign at approximately the same frequency (see Fig. 7). For OD75 and OP32 samples this conclusion is even more strict due to smaller bandwidth. Fig. 5 shows the results for Bi(Pb)-2212 OD75: (a) $\Sigma'(\omega)$ and $\Sigma''(\omega)$; (b) $k_m(\omega)$ and $\varepsilon(k)$ on top of the experimentally measured quasiparticle spectral weight.

The fact that ω_c is not equal but roughly two times less than $|\omega_0|$ is consistent with presence of an essential electron-electron scattering channel, the doping independent Auger like decay,[15] which originates from the electron-electron Coulomb interaction and which mainly determines the lifetime of quasiparticles at high frequencies.

C. Doping dependence of the renormalization

Another point arises as a consequence of the tight correlation between Σ' and Σ''. Recently we have shown[15] that two different channels can be distinguished in the scattering rate: the doping independent Auger-like decay, mentioned above, and the doping-dependent channel, which can be naturally associated with spin excitations. While such a decomposition of the scattering rate into two channels seems to be becoming commonly accepted,[19] there is still a controversy about the origin of the doping-dependent one. The present analysis shows that regardless of the nature of this channel, its doping and temperature dependence should appear in the doping and temperature dependence of Σ' and, consequently, of the renormalized dispersion, although it is clear that the variations in the latter should be marginal.

It is really so, and, in Fig. 6, we plot together the real parts of the self-energy for UD77 and OD75 samples at 130 K. Just from visual comparison of these data one can conclude that (i) the renormalization for UD77 is considerably higher than for OD75, (ii) the energy of the maximum of $\Sigma'(\omega)$ for the overdoped sample is lower than for the underdoped sample, it is about two times closer to the 70 meV "kink" energy, (iii) the kink feature is well defined in the underdoped case and becomes weaker with overdoping.

Following this tendency one can expect that with overdoping the 70 meV kink vanishes while the renormalization

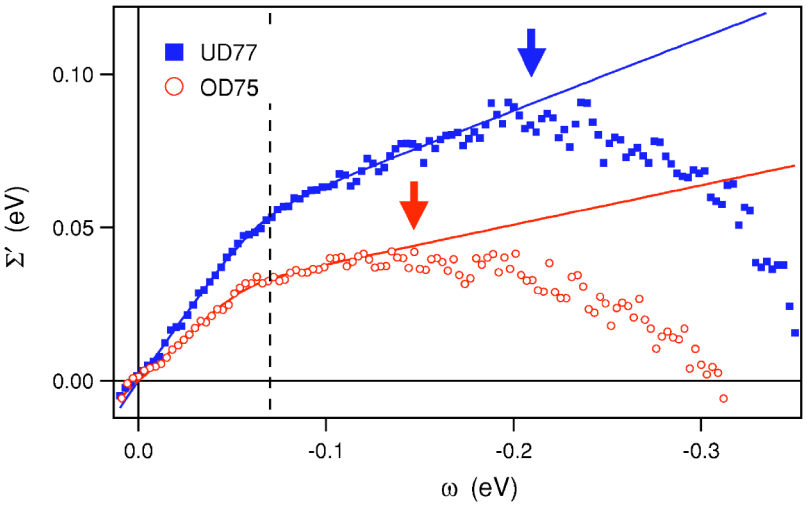

FIG. 6. (Color online.) The real parts of the self-energy for UD77 and OD75 samples at 130 K: solid lines show the result of fitting these real parts to Eq. (6) in a frequency range $0.17\ \mathrm{eV}<\omega<0$ for UD77 and $0.12\ \mathrm{eV}<\omega<0$ for OD75; looking down arrows mark $\Sigma'(\omega)$ maxima; the dashed line denotes the 70 meV "kink" energy.

maximum moves to lower frequencies faking a persistence of the kink in the whole doping range. Therefore, it is clear that in order to clarify the origin of the kink feature a quantitative measure of it is required.

D. Phenomenology of the kink

Keeping the visual definition of the kink as a sharp bend of the renormalized dispersion, we formalize it as a peak in the second derivative of $\Sigma'(\omega)$ and fitted it to a simple empirical function

$$\Sigma'_{\mathrm{low}}(\omega) = -\lambda\omega - \frac{\Delta\lambda}{\pi}(\omega-\omega_k) \times\left(\arctan\frac{\omega_k}{\delta}+\arctan\frac{\omega-\omega_k}{\delta}\right), \tag{6}$$

which gives a squared Lorentzian in a second derivative

$$K(\omega) = -\frac{d^2\Sigma'_{\mathrm{low}}(\omega)}{d\omega^2} = \frac{2}{\pi}\frac{\delta^3\Delta\lambda}{[\delta^2+(\omega-\omega_k)^2]^2}. \tag{7}$$

Fitting $\Sigma'(\omega)$ of the underdoped sample in $|\omega|<170$ meV energy range to this formula we have obtained an energy of the kink $\omega_k\approx-63$ meV, a kink width [half width at quarter maximum of $K(\omega)$] $\delta\approx30$ meV, and a strength of the kink $\int K d\omega=\Delta\lambda\approx0.65$. For the overdoped sample $\omega_k\approx-56$ meV, $\Delta\lambda\approx0.45$. We believe that a systematic study of this or similar quantitaties as a function of doping and temperature will help to find the origin of the main electronic interaction in superconducting cuprates.

V. CONCLUSIONS

We have demonstrated the full self-consistency of the data obtained using angle resolved photoemission and treated within the self-energy approach. The extracted bare band dispersion is in good agreement with the band structure calculations and allows one to quantify the self-energy of the electronic excitations in the real energy scale. The accurately determined real and imaginary parts of the self-energy prove the existence of well defined quasiparticles along the nodal direction even in the pseudogap state of Bi-2212.

The demonstrated self-consistency of the procedure opens a way to validate the photoemission spectra: the KK sieve can be used to verify the spectra for the absence of the band splitting or artificial features. The preliminary analysis of the spectra certified in such a way shows that the overall renormalization as well as kink in the nodal direction of Bi-based cuprates is highly doping dependent, decreasing with overdoping. In the light of the present dilemma about the origin of the main scattering boson in the cuprates, a systematic quantitative analysis of the KK verified spectra measured at different temperature and doping level is indispensable.

ACKNOWLEDGMENTS

The project is part of the Forschergruppe FOR538 and is supported by the DFG under Grants Nos. KN393/4 and 436UKR17/10/04 and by the Swiss National Science Foundation and its NCCR Network "Materials with Novel Electronic Properties." We are grateful to S. Ono and Yoichi Ando for supplying the Bi-2201 sample and A. Chubukov, I. Eremin, D. Manske, and V. Zabolotnyy for discussions.

APPENDIX

1. Kramers-Kronig transformation

The quasiparticle self-energy $\Sigma=\Sigma'+i\Sigma''$ in Eq. (1) is an analytical function the real and imaginary parts of which are related by the Kramers-Kronig (KK) transformation[20]

$$\Sigma'(\omega) = \frac{1}{\pi}\mathrm{PV}\int_{-\infty}^{\infty}\frac{\Sigma''(x)}{x-\omega}dx, \tag{A1}$$

$$\Sigma''(\omega) = -\frac{1}{\pi}\mathrm{PV}\int_{-\infty}^{\infty}\frac{\Sigma''(x)}{x-\omega}dx, \tag{A2}$$

where PV denotes the Cauchy principal value. It is instructive to express some interaction parameters via both self-energy functions. The coupling strength

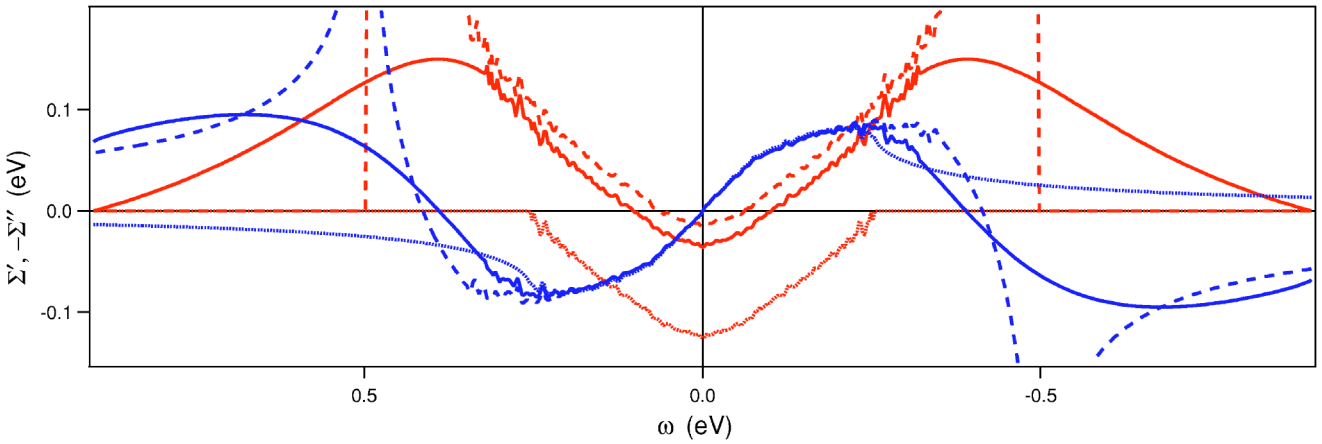

FIG. 7. (Color online.) Real (thin blue) and imaginary (thick red) parts of the self-energy related by Kramers-Kronig (KK) transform: $\Sigma' = \mathrm{KK}\Sigma''$, for three models of Σ'' tails.

$$\lambda = -\left(\frac{d\Sigma'}{d\omega}\right)_{\omega=0} \tag{A3}$$

can be expressed in terms of Σ'' differentiating the KK relation (A1):

$$\frac{d\Sigma'(\omega)}{d\omega} = \frac{1}{\pi}\mathrm{PV}\int_{-\infty}^{\infty}\frac{\Sigma''(x)-\Sigma''(\omega)}{(x-\omega)^2}dx. \tag{A4}$$

Here we use the fact that adding some constant to $\Sigma''(x)$ in Eq. (A1) does not change the result. Then, for an even $\Sigma''(\omega)$, Eq. (A4) leads to

$$\lambda = \frac{-2}{\pi}\mathrm{PV}\int_{0}^{\infty}\frac{\Sigma''(\omega)-\Sigma''(0)}{\omega^2}d\omega. \tag{A5}$$

2. Problem of tails

In order to illustrate the problem, we rewrite Eq. (A5) in an operator form $\lambda = -\mathbf{D}\Sigma''$ and express the parameters of the bare dispersion and renormalization via the experimental values of $v_R = (dk_m/d\omega)^{-1}_{\omega=0}$ and $\mathbf{D}W$: e.g., $v_F^{-1} = v_R^{-1} - \mathbf{D}W$, or $\lambda = 1/Z - 1$, where

$$Z = 1 - v_R\mathbf{D}W \tag{A6}$$

is the coherence factor $(0 < Z < 1)$. In case the MDC width $W(\omega)$ decays to zero or saturates on the scale covered by experiment, as it is expected for the scattering by phonons,[21] the $\mathbf{D}W$ value can be easily defined, and all the mentioned parameters can be derived from experimental value of v_R and $W(\omega)$ function. In cuprates, however, $W(\omega)$, along the nodal direction, does not decrease or even saturate in the whole experimentally accessible energy region (up to $\omega_m = 0.5$ eV).

Equation (A5) can give a certain feeling how the high-energy tails of the scattering rate $\Sigma''(\omega)$ for $|\omega| > \omega_m$ influences λ. For example, for a simple case

$$\Sigma''(\omega) = -\begin{cases} \alpha\omega^2 + C & \text{for } |\omega| < \omega_c, \\ 0 & \text{for } |\omega| > \omega_c, \end{cases} \tag{A7}$$

where $\omega_c > 0$ is an energy cutoff and $C \equiv -\Sigma''(0) > 0$ is an offset, Eq. (A5) gives

$$\lambda = \frac{2}{\pi}\left(\alpha\omega_c - \frac{C}{\omega_c}\right) \approx \frac{2}{\pi}\alpha\omega_c \tag{A8}$$

for $C \ll \omega_c$. Using another ultimate model for Σ'' tails,

$$\Sigma''(\omega) = -\begin{cases} \alpha\omega^2 + C & \text{for } |\omega| < \omega_c, \\ \alpha\omega_c^2 + C & \text{for } |\omega| > \omega_c, \end{cases} \tag{A9}$$

which approximates the saturation of scattering rate at high frequencies, one obtains $\lambda = 4\alpha\omega_c/\pi$, twice of Eq. (A8). In the following sections we show how we solve this problem.

3. Calculation of Σ'_{KK}

In order to perform a KK transform, high-energy tails should be attached to $\Sigma''(\omega)$ derived from Eq. (5). Equations (A7) and (A9) represent two extremes which can be enclosed in a simple analytical expression

$$\Sigma''_{\mathrm{mod}}(\omega) = -\frac{\alpha\omega^2 + C}{1 + \left|\dfrac{\omega}{\omega_c}\right|^n}, \tag{A10}$$

as the ultimate cases with $n \to \infty$ and $n = 2$, respectively. For given n and ω_c, we construct $\Sigma''(\omega)$ function in a wide frequency range (up to $|\omega_0|$ or higher) assuming the particle-hole symmetry

$$\Sigma''(\omega) = \begin{cases} \Sigma''_{\mathrm{width}}(|\omega|) & \text{for } |\omega| < \omega_m, \\ \Sigma''_{\mathrm{mod}}(\omega) & \text{for } |\omega| > \omega_m, \end{cases} \tag{A11}$$

where ω_m is a "confidence limit," a maximal experimental binding energy to which both the $W(\omega)$ and $k_m(\omega)$ functions can be confidently determined, $\Sigma''_{\mathrm{width}}(\omega)$ is calculated from Eqs. (5) for given ω_0, and $\Sigma''_{\mathrm{mod}}(\omega)$ is fitted to $\Sigma''_{\mathrm{width}}(\omega)$ in the confidence range in order to define α and C. Then, $\Sigma'_{\mathrm{KK}}(\omega)$ is obtained from $\Sigma''(\omega)$ by KK transform (A1).

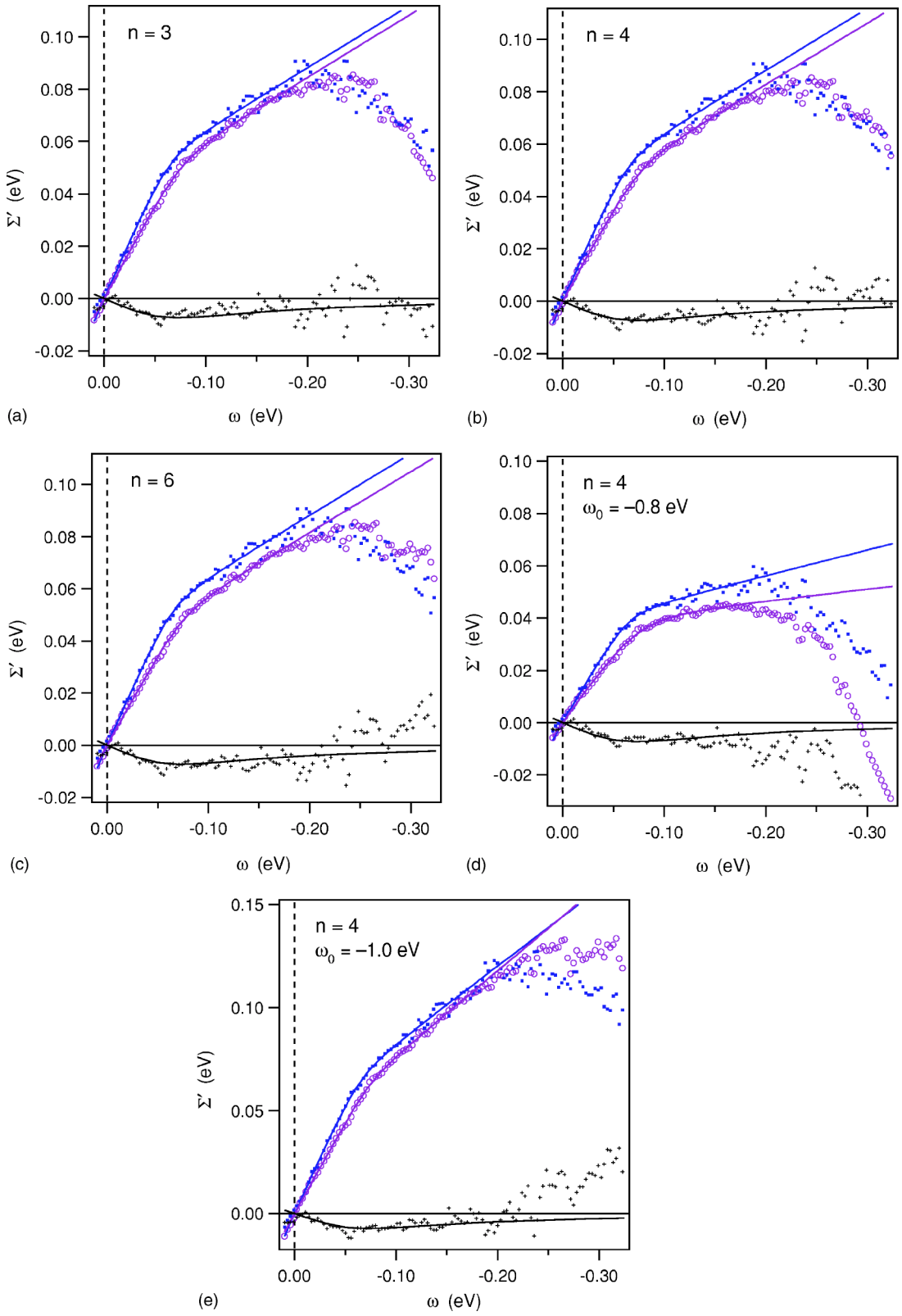

FIG. 8. (Color online.) Illustration of the fitting procedure: real parts of the self-energy $\Sigma'_{\mathrm{disp}}(\omega)$ (filled squares) obtained by (4) and $\Sigma'_{\mathrm{KK}}(\omega)$ (open circles) by Eqs. (5) and (A1); the difference $\Delta\Sigma'(\omega)=\Sigma'_{\mathrm{KK}}(\omega)-\Sigma'_{\mathrm{disp}}(\omega)$ (small crosses) is fitted to $R'(\omega)$ (corresponding solid line), the contribution of overall resolution determined by Eqs. (A12) and (A13). In the first three panels $\omega_0=-0.9$ but different $n=3$, 4, and 6 in Eq. (A10) are compensated by different $\omega_c=0.34$, 0.45, and 0.52 eV, respectively. The last two panels, the "best" fitting results for slightly different ω_0's.

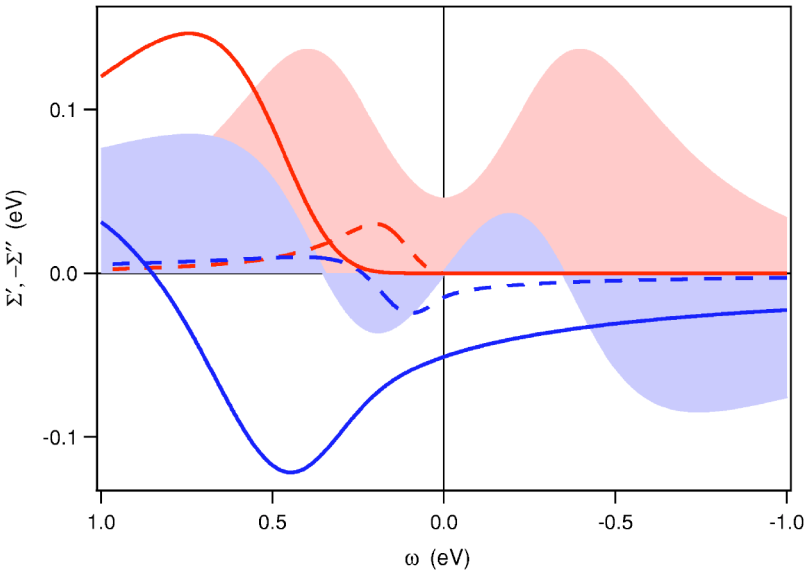

FIG. 9. (Color online.) Possible particle-hole asymmetry effect on $\Sigma''(\omega)$ (red/thick lines) and $\Sigma'(\omega)$ (blue/thin lines): low-energy (dashed lines, $\omega_c=0.1$ eV) and high-energy [solid lines, by Eq. (A14)] contributions shown on the top of the symmetric self-energy (shaded areas).

Figure 7 shows the pairs of $\Sigma''(\omega)$ and $\Sigma'(\omega)$ functions obtained in such a way for the same ω_0 but for three different models: Eqs. (A7), (A9), and (A10) with $n=4$ (dashed, dotted, and solid lines, respectively). Since $\mathrm{KK}C=0$, in order to simplify numerical calculation, the offset of $\Sigma''(\omega)$ curves is set to $\Sigma''(\omega_0)=0$. The experimental data are taken for UD77 sample.

4. Resolution function

In step (iii), as we mentioned above, the difference $\Delta\Sigma'(\omega)=\Sigma'_{\mathrm{KK}}(\omega)-\Sigma'_{\mathrm{disp}}(\omega)$ should be fitted not to zero but to some small but detectable contribution of the overall resolution $R'(\omega)$. This difference can be easily understood by reasoning that finite energy and angular resolutions mainly effect the MDC's width rather than its peak position and that its contribution is frequency dependent. In order to illustrate this we can take into account the overall resolution, R, as $\Sigma''_{\mathrm{width}}(\omega)=\sqrt{\Sigma''(\omega)^2+R^2}$. Then one can consider its frequency-dependent contribution to the imaginary part of $\Sigma(\omega)$ as the difference between $\Sigma''_{\mathrm{width}}(\omega)$ and real $\Sigma''(\omega)$:

$$R''(\omega)=\sqrt{R^2+\Sigma''(\omega)^2}-\Sigma''(\omega), \tag{A12}$$

and, due to additivity of the KK transform, $\Sigma'_{\mathrm{KK}}=\mathrm{KK}\Sigma''_{\mathrm{width}}=\mathrm{KK}\Sigma''+\mathrm{KK}R''=\Sigma'_{\mathrm{disp}}+R'$, construct ω-dependent contribution to Σ'_{KK} as

$$R'(\omega)=\mathbf{KK}R''(\omega). \tag{A13}$$

Although, in principle, the resolution effect $R'(\omega)$ can be explicitely calculated from known energy and momentum resolutions, here we derive it empirically using R as a parameter. It is seen from Fig. 7 that different tails do not affect the energy region $|\omega|<0.25$ eV, so, an irreducible difference in the slopes (see Fig. 8) $\Delta=d\Sigma'_{\mathrm{KK}}(\omega)/d\omega-d\Sigma'_{\mathrm{disp}}(\omega)/d\omega>0$ in the low-energy range $|\omega|<0.07$ eV (while $\Delta=0$ at higher energies 0.1 eV$<|\omega|<0.2$ eV) is a measure of $R'(\omega)$.

In Fig. 8 we plot $R'(\omega)$ setting the offset of $\Sigma''(\omega)$ to zero that gives the value of $R=0.015$ eV. For $\Sigma''(0)<0$ the procedure gives larger R values to accommodate the difference in slopes but this does not affect the fact that the irreducible difference between $\Sigma'_{\mathrm{KK}}(\omega)$ and $\Sigma'_{\mathrm{disp}}(\omega)$ is caused by the experimental resolution, and depends on frequency as is shown in Fig. 8: it vanishes at zero and high frequencies having a maximum around 0.1 eV.

Thus, we can visualize the fitting procedure as fitting the difference $\Delta\Sigma'(\omega)$ to $R'(\omega)$ function. The procedure has appeared to be robust with respect to the ω_0 determination. Figure 8 illustrates this. First three panels show that for a correct value of $\omega_0=-0.9$ eV there is space for other parameters to vary: different tails can be compensated by different ω_c's, e.g., for $n=3$, 4, and 6 in Eq. (A10), $\omega_c=0.34$, 0.45, and 0.52 eV, respectively. On the other hand, at slightly different ω_0's (about 10% lower and higher, see two right panels), $\Delta\Sigma'(\omega)$ cannot be fitted to $R'(\omega)$ in the whole frequency range.

5. Model assumptions

Finally, we discuss two assumptions which have been made about the model self-energy: k-independence and particle-hole symmetry. It has been mentioned above that the symmetric Lorentzian line shape of the MDC's taken along the nodal direction was considered as an experimental evidence that the quasiparticle self-energy hardly depends on momentum.[5] Recently, however, it has been noticed that the necessary condition for the Lorentzian line shape is $\partial\Sigma''(k,\omega)/\partial k=0$, but $\partial\Sigma'/\partial k$ can be an ω-independent constant.[22] This is especially interesting because the authors of Ref. 22 have shown that such a linear k-dependence of Σ' can explain a nontrivial doping-dependent high-energy dispersion observed for a variety of cuprates.[23]

As long as $\Sigma'(k,\omega)=\Sigma'_k(k)+\Sigma'_\omega(\omega)$ and $\partial\Sigma''/\partial k=0$, k dependence of Σ' does not affect any result of the presented analysis except the bare dispersion. In this case, the real bare dispersion is just $\varepsilon^{\mathrm{real}}(k)=\varepsilon(k)-\Sigma'_k(k)$ or $v_F^{\mathrm{real}}=v_F-(\partial\Sigma'/\partial k)_{k=k_F}$. Although our preliminary results, being in agreement with band structure calculations[12] and experimen-

tal plasmon dispersion,[13] do not support strong k dependence of Σ', it will be interesting to examine its possible contribution in a wide doping range and for different compounds.

A possible particle-hole asymmetry is another complication which can effect the results of the presented analysis. In general, one can expect an asymmetry of the self-energy due to an asymmetric electron-boson interaction or as a simple consequence of asymmetric density of states. Without considering the origin of the asymmetry, we examine its possible influence based on the energy scale where it can appear. It is well known that because of the possibility to perform ARPES at finite temperature one can get the information about quasiparticle spectral weight not only below the chemical potential but also from some region above.[24] For $T=300$ K the MDC width can be measured up to 50 meV above E_F, and, within the experimental uncertainty, it has appeared to be completely symmetric (e.g., see Ref. 15). This means that if there is some asymmetry in the scattering rate at low-energy scale ($\sim$0.1 eV, a characteristic scale which can originate from an electron-boson interaction or from the van Hove singularity in the occupied density of states of the hole-doped cuprates), its magnitude is too small to be seen in the $|\omega|<50$ meV energy range and, consequently, hardly effects the quasiparticle renormalization in the occupied region ($\omega<0$). Figure 9 illustrates this: the dashed curves, on top of the symmetric self-energy shown by shaded areas, represent a low-energy asymmetric contribution which is too big not to be noticed in $\Sigma''(\omega)$ (for $|\omega|<50$ meV) but too small to influence $\Sigma'(\omega<0)$.

The solid curves in Fig. 9 present the case of high-energy asymmetry that can steam from the asymmetry of the bare band.[9] We simulate it by an asymmetry part in the scattering rate

$$\Sigma''_a(\omega)=\begin{cases}\Sigma''_{\mathrm{mod}}(\omega,\omega_{c2})-\Sigma''_{\mathrm{mod}}(\omega,\omega_c), & \omega>0,\\ 0, & \omega<0,\end{cases} \tag{A14}$$

where Σ''_{mod} is determined by Eq. (A10) with $\omega_c=0.45$ eV, $\omega_{c2}=0.66$ eV, $n=4$, $C=0$. It is seen that although the influence of $\Sigma'_a(\omega)$ on renormalization at -0.5 eV$<\omega<0$ eV is rather small (can be approximated at this stage by a linear contribution with a slope of about 20% of λ) it can be, in principle, detected by more precise analysis, in which the influence of the energy and angular resolutions is taken into account explicitly.

[1] A. Damascelli, Z.-X. Shen, and Z. Hussain, Rev. Mod. Phys. **75**, 473 (2003).

[2] J. C. Campuzano, M. R. Norman, and M. Randeria, in *Physics of Conventional and Unconventional Superconductors*, edited by K. H. Bennemann and J. B. Ketterson (Springer-Verlag, Berlin, 2004), Vol. 2.

[3] T. Valla, A. V. Fedorov, P. D. Johnson, B. O. Wells, S. L. Hulbert, Q. Li, G. D. Gu, and N. Koshizuka, Science **285**, 2110 (1999).

[4] P. V. Bogdanov, A. Lanzara, S. A. Kellar, X. J. Zhou, E. D. Lu, W. J. Zheng, G. Gu, J.-I. Shimoyama, K. Kishio, H. Ikeda, R. Yoshizaki, Z. Hussain, and Z. X. Shen, Phys. Rev. Lett. **85**, 2581 (2000).

[5] A. Kaminski, M. Randeria, J. C. Campuzano, M. R. Norman, H. Fretwell, J. Mesot, T. Sato, T. Takahashi, and K. Kadowaki, Phys. Rev. Lett. **86**, 1070 (2001).

[6] S. V. Borisenko, A. A. Kordyuk, S. Legner, C. Dürr, M. Knupfer, M. S. Golden, J. Fink, K. Nenkov, D. Eckert, G. Yang, S. Abell, H. Berger, L. Forró, B. Liang, A. Maljuk, C. T. Lin, and B. Keimer, Phys. Rev. B **64**, 094513 (2001).

[7] A. A. Abrikosov, L. P. Gor'kov, and I. E. Dzyaloshinskii, *Quantum Field Theoretical Methods in Statistical Physics* (Pergamon, Oxford, 1965).

[8] P. D. Johnson, T. Valla, A. V. Fedorov, Z. Yusof, B. O. Wells, Q. Li, A. R. Moodenbaugh, G. D. Gu, N. Koshizuka, C. Kendziora, Sha Jian, and D. G. Hinks, Phys. Rev. Lett. **87**, 177007 (2001).

[9] A. A. Kordyuk, S. V. Borisenko, M. Knupfer, and J. Fink, Phys. Rev. B **67**, 064504 (2003).

[10] A. Koitzsch, S. V. Borisenko, A. A. Kordyuk, T. K. Kim, M. Knupfer, J. Fink, H. Berger, and R. Follath, Phys. Rev. B **69**, 140507(R) (2004).

[11] O. K. Andersen, A. I. Liechtenstein, O. Jepsen, and F. Paulsen, J. Phys. Chem. Solids **56**, 1573 (1995).

[12] A. A. Kordyuk, S. V. Borisenko, A. N. Yaresko, S.-L. Drechsler, H. Rosner, T. K. Kim, A. Koitzsch, K. A. Nenkov, M. Knupfer, J. Fink, R. Follath, H. Berger, B. Keimer, S. Ono, and Yoichi Ando, Phys. Rev. B **70**, 214525 (2004).

[13] N. Nücker, U. Eckern, J. Fink, and P. Müller, Phys. Rev. B **44**, 7155 (1991); V. G. Grigoryan, G. Paasch, and S.-L. Drechsler, *ibid.* **60**, 1340 (1999).

[14] T. K. Kim, A. A. Kordyuk, S. V. Borisenko, A. Koitzsch, M. Knupfer, H. Berger, and J. Fink, Phys. Rev. Lett. **91**, 167002 (2003).

[15] A. A. Kordyuk, S. V. Borisenko, A. Koitzsch, J. Fink, M. Knupfer, B. Büchner, H. Berger, G. Margaritondo, C. T. Lin, B. Keimer, S. Ono, and Yoichi Ando, Phys. Rev. Lett. **92**, 257006 (2004).

[16] S. V. Borisenko, A. A. Kordyuk, S. Legner, T. K. Kim, M. Knupfer, C. M. Schneider, J. Fink, M. S. Golden, M. Sing, R. Claessen, A. Yaresko, H. Berger, C. Grazioli, and S. Turchini, Phys. Rev. B **69**, 224509 (2004).

[17] For comparison of the offset value to transport data see T. Yoshida, X. J. Zhou, H. Yagi, D. H. Lu, K. Tanaka, A. Fujimori, Z. Hussain, Z.-X. Shen, T. Kakeshita, H. Eisaki, S. Uchida, Kouji Segawa, A. N. Lavrov, and Yoichi Ando, Physica B **351**, 250 (2004).

[18] C. M. Varma, P. B. Littlewood, S. Schmitt-Rink, E. Abrahams, and A. E. Ruckenstein, Phys. Rev. Lett. **63**, 1996 (1989).

[19] X. J. Zhou, Junren Shi, T. Yoshida, T. Cuk, W. L. Yang, V. Brouet, J. Nakamura, N. Mannella, Seiki Komiya, Yoichi Ando, F. Zhou, W. X. Ti, J. W. Xiong, Z. X. Zhao, T. Sasagawa, T. Kakeshita, H. Eisaki, S. Uchida, A. Fujimori, Zhenyu Zhang, E. W. Plummer, R. B. Laughlin, Z. Hussain, and Z.-X. Shen, cond-mat/0405130 (unpublished).

[20] L. D. Landau and E. M. Lifschitz, *Statistical Physics* (Pergamon,

Oxford, 1980), Pt. 1.
[21] T. Valla, A. V. Fedorov, P. D. Johnson, and S. L. Hulbert, Phys. Rev. Lett. **83**, 2085 (1999).
[22] M. Randeria, A. Paramekanti, and N. Trivedi, Phys. Rev. B **69**, 144509 (2004).
[23] X. J. Zhou, T. Yoshida, A. Lanzara, P. V. Bogdanov, S. A. Kellar, K. M. Shen, W. L. Yang, F. Ronning, T. Sasagawa, T. Kakeshita, T. Noda, H. Eisaki, S. Uchida, C. T. Lin, F. Zhou, J. W. Xiong, W. X. Ti, Z. X. Zhao, A. Fujimori, Z. Hussain, and Z.-X. Shen, Nature (London) **423**, 398 (2003).
[24] T. Sato, T. Kamiyama, T. Takahashi, J. Mesot, A. Kaminski, J. C. Campuzano, H. M. Fretwell, T. Takeuchi, H. Ding, I. Chong, T. Terashima, and M. Takano, Phys. Rev. B **64**, 054502 (2001).